TECTONICS, VOL. 32, 1371–1383, doi:10.1002/tect.20084, 2013

Tracking the Australian plate motion through the Cenozoic: Constraints from $^{40}Ar/^{39}Ar$ geochronology

Benjamin E. Cohen,[1,2] Kurt M. Knesel,[1] Paulo M. Vasconcelos,[1] and Wouter P. Schellart[3]

Received 2 April 2013; revised 26 August 2013; accepted 12 September 2013; published 3 October 2013.

[1] Here we use geochronology of Australian intraplate volcanoes to construct a high-resolution plate-velocity record and to explore how tectonic events in the southwest Pacific may have influenced plate motion. Nine samples from five volcanoes yield ages from 33.6 ± 0.5 to 27.3 ± 0.4 Ma and, when combined with published ages from 30 to 16 Ma, show that the rate of volcanic migration was not constant. Instead, the results indicate distinct changes in Australian plate motion. Fast northward velocities (61 ± 8 and 57 ± 4 km/Ma) prevailed from 34 to 30 (±0.5) and from 23 to 16 (±0.5) Ma, respectively, with distinct reductions to 20 ± 10 and 22 ± 5 km/Ma from 30 to 29 (±0.5) Ma and from 26 to 23 (±0.5) Ma. These velocity reductions are concurrent with tectonic collisions in New Guinea and Ontong Java, respectively. Interspersed between the periods of sluggish motion is a brief 29–26 (±0.5) Ma burst of atypically fast northward plate movement of 100 ± 20 km/Ma. We evaluate potential mechanisms for this atypically fast velocity, including catastrophic slab penetration into the lower mantle, thermomechanical erosion of the lithosphere, and plume-push forces; none are appropriate. This period of fast motion was, however, coincident with a major southward propagating slab tear that developed along the northeastern plate margin, following partial jamming of subduction and ophiolite obduction in New Caledonia. Although it is unclear whether such an event can play a role in driving fast plate motion, numerical or analogue models may help address this question.

Citation: Cohen, B. E., K. M. Knesel, P. M. Vasconcelos, and W. P. Schellart (2013), Tracking the Australian plate motion through the Cenozoic: Constraints from $^{40}Ar/^{39}Ar$ geochronology, *Tectonics*, *32*, 1371–1383, doi:10.1002/tect.20084.

1. Introduction

[2] Subduction zones are the most complex tectonic environments on Earth. This is exemplified by the dynamic subduction systems in the southwest Pacific (Figure 1), which, during the Cenozoic, have undergone numerous episodes of collisional orogenesis, slab rollback, slab tearing, initiation of new subduction zones, and subduction polarity reversal [*Petterson et al*., 1997, 1999; *Hall*, 2002; *Sdrolias et al*., 2003; *Cowley et al*., 2004; *Kroenke et al*., 2004; *Quarles van Ufford and Cloos*, 2005; *Schellart et al*., 2006]. One of the major goals of modern geodynamics is to constrain the timing and duration for changes in subduction dynamics. Reconstructing subduction history can be challenging, however, as subduction terrains are often located in remote, rugged, vegetated, or submarine areas; subsequent tectonism may overprint earlier episodes, or the evidence is destroyed when terrains are subducted. Nevertheless, a powerful approach to determine the age and duration of tectonic events, including within subduction zones, is the reconstruction of paleoplate velocities as recorded by deviations in the geometry and age progression of plume-derived intraplate volcanic chains [e.g., *Müller et al*., 1993; *Sharp and Clague*, 2006; *Whittaker et al*., 2007; *Wessel and Kroenke*, 2009; *Ray et al*., 2012]. Although this approach is most commonly applied to oceanic hot spots, recent geochronological studies of intraplate volcanoes in eastern Australia [*Cohen et al*., 2007; *Knesel et al*., 2008] have demonstrated that in some cases, the method works equally well for continental hot spots.

[3] A long record of Australian plate motion is provided by hot spot–derived volcanoes extending over 1800 km along the eastern margin of the continent [*Wellman and McDougall*, 1974]. The age-progressive nature of the volcanism was first recognized from K-Ar analysis which provided strong evidence for motion of the Australian plate over a mantle hot spot [*Wellman and McDougall*, 1974]. This hot spot volcanism is chemically bimodal, with silicic plugs and flows concentrated in the cores of variably eroded shields of mafic lavas. Because the silicic magmas were emplaced over relatively brief periods of 1 Ma or less, toward the end of mafic activity, they provide an opportunity to develop a high-resolution geospeedometer for the Australian plate [*Cohen et al*., 2007; *Knesel et al*., 2008]. In a systematic approach, we demonstrated that $^{40}Ar/^{39}Ar$ dating of these

Additional supporting information may be found in the online version of this article.

[1]School of Earth Sciences, The University of Queensland, Brisbane, Qld, Australia.

[2]Now at NERC Argon Isotope Facility, Scottish Universities Environmental Research Centre, East Kilbride, UK.

[3]School of Geosciences, Monash University, Clayton Campus, Melbourne, Vic, Australia.

Corresponding author: B. E. Cohen, NERC Argon Isotope Facility, Scottish Universities Environmental Research Centre, Rankine Ave., East Kilbride G75 0QF, UK. (ben.cohen@glasgow.ac.uk)

0278-7407/13/10.1002/tect.20084

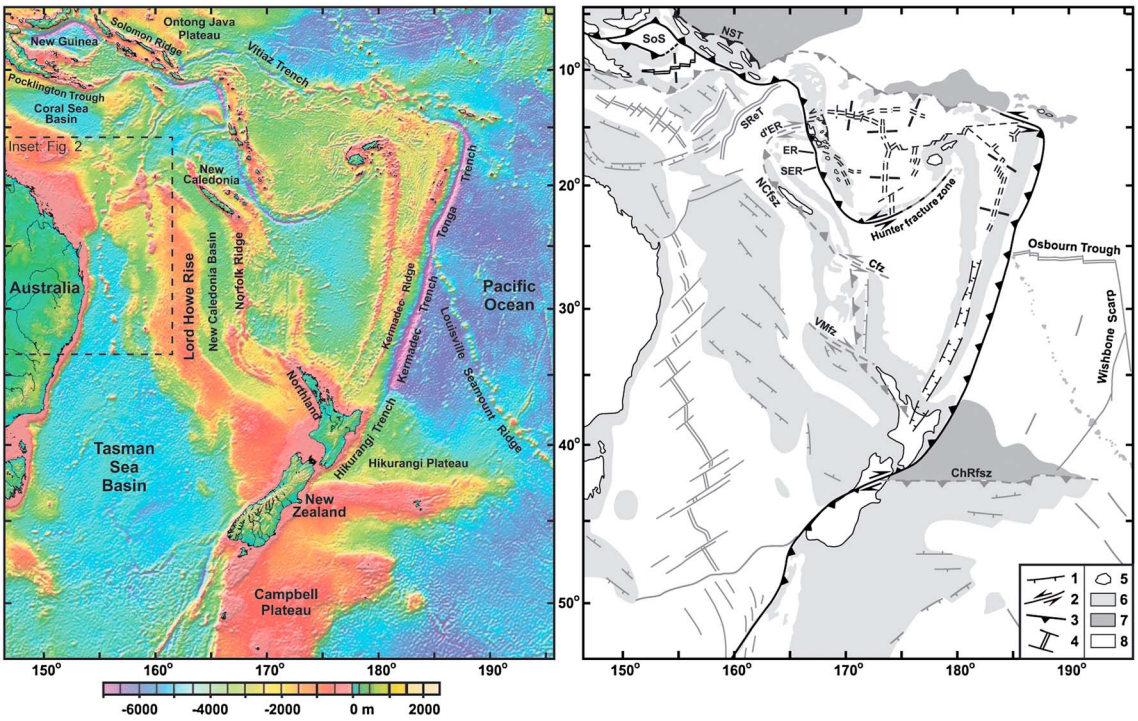

Figure 1. Present-day tectonic elements of the southwest Pacific, after *Schellart et al*. [2006]. Dashed box shows the location of Figure 2. Abbreviations are as follows: SoS, Solomon Sea; NST, North Solomon Trough; SReT, South Rennel Trough; d'ER, d'Entrecasteaux Ridge; NCfsz, New Caledonia fossil subduction zone; ER, Efate Re-entrant; SER, South Efate Re-entrant; Cfz, Cook fracture zone; VMfz, Vening Meinesz fracture zone; ChRfsz, Chatham Rise fossil subduction zone. 1, normal fault; 2, strike-slip fault; 3, subduction zone; 4, spreading ridge (double line) and transform faults (single lines); 5, land; 6–8, sea, with 6, continental or arc crust; 7, oceanic plateau; and 8, basin/ocean floor. Structures in light grey indicate former Cenozoic features that have become inactive.

silicic volcanic and hypabyssal rocks provides a tool for tracking volcanic migration rates over periods as brief as a few million years [*Cohen et al*., 2007] and, when applied on a regional scale, provides an avenue to identify and constrain abrupt variations in motion of the Australian plate [*Knesel et al*., 2008]. Here we extend and refine this record of plate motion through $^{40}Ar/^{39}Ar$ analysis of the five additional hot spot volcanoes on the Australian continent (Figure 2). The ages from this paper, when combined with our previous results [*Cohen et al*., 2007; *Knesel et al*., 2008], define a record of Australian intraplate volcanism and plate velocity from 34 Ma until 16 Ma. We then use this record to constrain the timing and duration of tectonic events in the southwest Pacific region, particularly collisions in the New Guinea, New Caledonia, and Ontong Java regions, where the ages of collision have proven difficult to constrain. We also find evidence for a period from 29 to 26 (±0.5) Ma of atypically fast plate velocity that correlates with a slab tear event in the region. We then use the accurate timing of the atypically fast plate velocity combined with the regional tectonic setting of the Australian plate to provide constraints on the driving mechanism that might have been responsible for such rapid motion.

2. Material and Methods

[4] Sample selection, preparation, and $^{40}Ar/^{39}Ar$ methodologies are identical to those in *Cohen et al*. [2007] and *Knesel et al*. [2008]. To facilitate comparison with our previously published ages for east Australian volcanism [*Cohen et al*., 2007, 2008; *Knesel et al*., 2008], we use the decay constants and atmospheric value of *Steiger and Jäger* [1977] and the Fish Canyon sanidine age of *Renne et al*. [1998] rather than the recently revised values of *Lee et al*. [2006], *Kuiper et al*. [2008], or *Renne et al*. [2010]. If the analyses are recalculated based on the revised constants, then the ages become approximately 0.2 Ma older. Age uncertainties are reported at the 95% confidence level (2σ) and include the errors in the irradiation correction factors and the error in the irradiation parameter J. The reported errors do not include the uncertainty in the potassium decay constants [*Min et al*., 2000]. Plateaus were calculated if three or more contiguous steps, which comprised more than 50% of the total ^{39}Ar released for that sample, overlapped within the 95% confidence interval [*Fleck et al*., 1977].

[5] The retrieval of potassium-rich phenocrysts, especially sanidine and biotite, improves the precision and accuracy of the geochronological results relative to analysis of groundmass material. Petrographic inspection indicates that many of these crystals within each of the dated samples are fresh and unaltered (Figure 3). The visibly fresh crystals were selected for geochronology by handpicking under a binocular microscope. In the case of sanidine and K-feldspar samples, only transparent crystals were selected, avoiding fluid inclusions, solid inclusions, or adhering groundmass. In one case (BC-94, anorthoclase), crystals with areas of iron-staining and minor inclusions of clinopyroxene or magnetite were

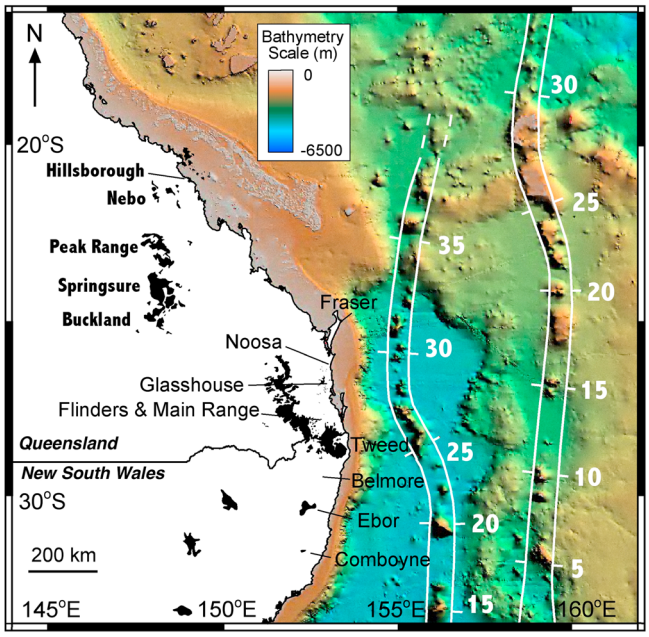

Figure 2. Distribution of hot spot–derived intraplate volcanism on the Australian plate, modified after *Knesel et al.* [2008]. Volcanoes in bold are those analyzed here; normal font indicates those dated previously [*Ashley et al.*, 1995; *Cohen et al.*, 2007; *Knesel et al.*, 2008]. Numbers in white to the right of the two seamount trails are calculated ages [*Knesel et al.*, 2008].

selected as these features were unavoidable. Nevertheless, the clinopyroxene, magnetite, and iron-staining phases are not potassium bearing, so they should not influence K or Ar distribution within the crystals. The biotite crystals selected were free from visible signs of alteration, while the groundmass sample (BC-95r) was from a well-crystallized rock containing feldspar, arfvedsonite, and quartz.

[6] A total of nine samples dated from the Hillsborough-Buckland lineament of volcanoes in central and northern Queensland, representing the northernmost exposed hot spot–derived volcanoes on the Australian continent. Typically, one silicic sample was dated per volcano (at Hillsborough, Nebo, Springsure, and Buckland), with three samples at North Peak Range and two samples at South Peak Range (Table 1 and Figure 2). Of these nine samples, five (comprising three feldspar separates, one biotite separate, and one groundmass separate) were dated via the incremental-heating technique (Figure 4). Feldspar crystals for incremental heating were obtained from an alkaline granite intrusion from Hillsborough, a trachyandesite lava flow from North Peak Range, and a metaluminous trachyte in South Peak Range. The biotite and groundmass separates were also obtained from units in North Peak Range and South Peak Range, from peraluminous and peralkaline rhyolite plugs, respectively. Phenocrystic sanidine crystals for total-fusion analysis were separated from five samples: a rhyolite dyke in the Nebo volcano, two peraluminous rhyolite plugs from North Peak Range, a crystal-rich pitchstone plug from Springsure, and a peralkaline trachyte plug from Buckland (Figure 5 and Table A1 in the supporting information). As a cross-check of the total-fusion and incremental-heating analyses on different phases, we analyzed both biotite (via incremental heating) and sanidine (via total fusion) for a peraluminous rhyolite from North Peak Range (BC-89) (Figures 3 and 4 and Table 1).

3. Results

3.1. Incremental-Heating Analyses

[7] For the five samples analyzed via incremental heating, duplicate analyses from each sample provide an independent test on the reliability of the results (Figure 4). Plateaus extend over most (73–100%) of the ^{39}Ar released, indicating near-ideal sample behavior with little or no signs of argon loss or excess argon (Figure 4 and Table 1). Here we discuss the incremental-heating results in order from north to south.

[8] In the case of K-feldspar from Hillsborough (BC-98, Figures 4a and 4b), plateaus extend over 100% and 96.9% of the ^{39}Ar released, and all steps have high and uniform ^{40}Ar* and K/Ca values, indicating the reliability of the results. The best age estimate for this sample of 33.6 ± 0.5 Ma was determined from the mean-weighted age on the age probability spectrum.

[9] Farther south, biotite from a peraluminous rhyolite plug from North Peak Range (BC-89, Figures 4c–4e) also yielded flat spectra, with plateaus covering 92.8% and 100% of the gas released. The two plateau ages of 30.8 ± 0.4 and 30.4 ± 0.5 Ma are indistinguishable from each other and from the isochron age of 30.6 ± 0.4 Ma, indicating that the biotite has remained a closed system since eruption (Figures 4c–4e). The initial ^{40}Ar/^{36}Ar value is also within error from the present-day atmosphere, indicating that this biotite does not host excess argon (Figure 4e).

[10] The two K-feldspar crystals from a trachyandesite flow in North Peak Range (BC-90) yielded excellent plateaus, comprising 98.2% and 100% of the ^{39}Ar released (Figures 4f and 4g and Table 1). Plateau ages are indistinguishable at 30.4 ± 0.5 and 30.9 ± 1.1 Ma, with the first grain being considerably larger and yielding correspondingly higher quantities of gas and more precise results (Tables 1 and A2). The isochron age, combining results from both grains analyzed, yields an indistinguishable age to the plateaus, and the initial ^{40}Ar/^{36}Ar is within error from the modern-day atmospheric value (Figure 4h).

[11] The duplicate anorthoclase analyses from BC-94 (a metaluminous trachyte plug from South Peak Range) are also highly reproducible, with both grains yielding very precise analyses and plateaus covering 100% of the gas released (Figures 4i and 4j). Again, both plateau ages (28.9 ± 0.4 Ma and 29.0 ± 0.4 Ma) are indistinguishable from each other and from the combined isochron age of 29.0 ± 0.4 Ma (Figure 4k), indicating that these results are a reliable estimate for the cooling age of this intrusion.

[12] Incremental heating of the peralkaline groundmass sample (BC-95r) from South Peak Range reveals minor signs of possible excess argon or recoil within this sample, with the lowest-temperature steps having older ages than the plateaus (Figures 4l and 4m). The presence of excess argon is supported by the isochron, which yields a single linear array, but with the initial ^{40}Ar/^{36}Ar value of 317 ± 6, outside error from the atmospheric value of 295.5 (Figure 4n). Despite the presence of this minor excess argon component, the plateau ages for this sample are concordant with the isochron

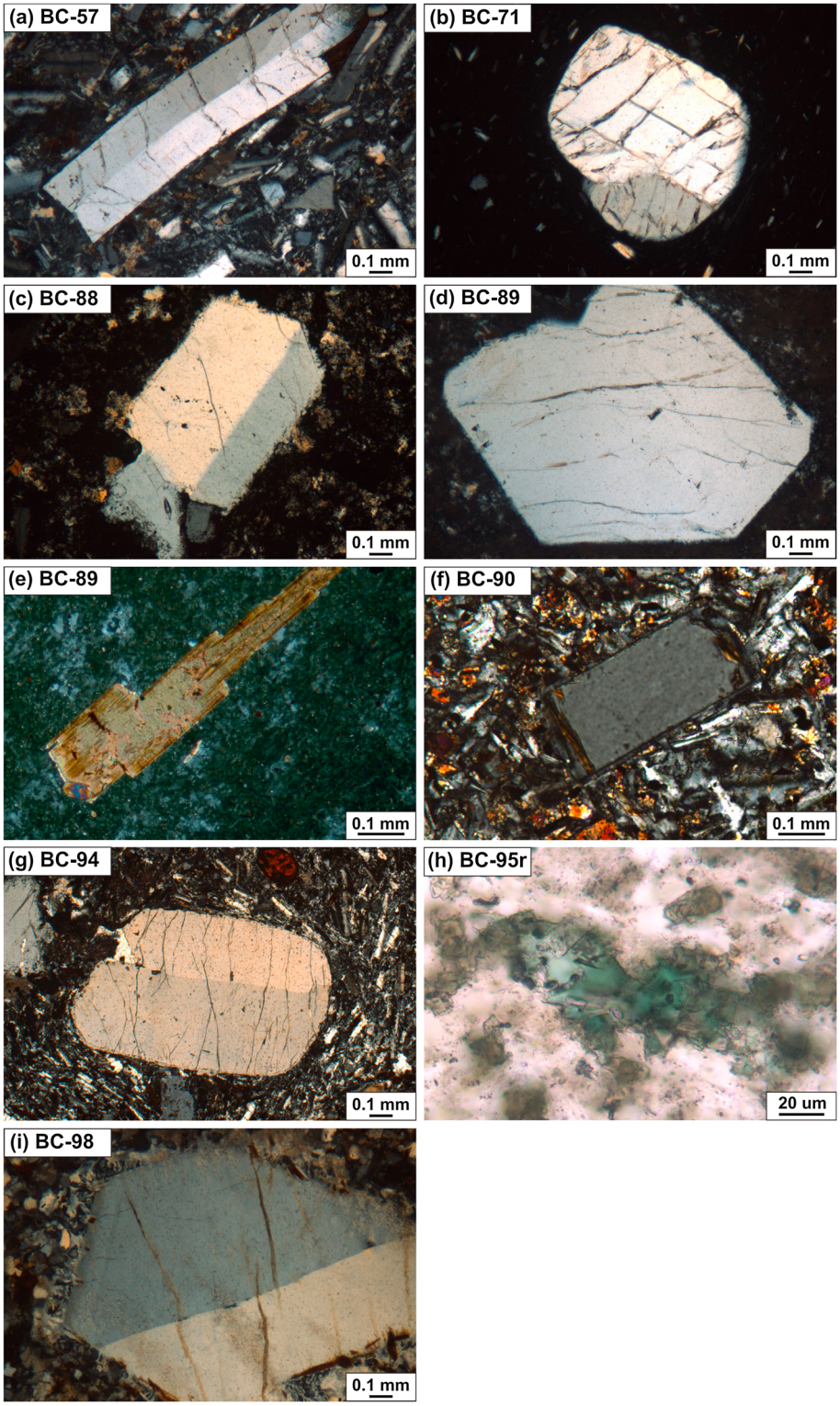

Figure 3. Representative petrographic images of the phases analyzed by $^{40}Ar/^{39}Ar$ geochronology. (a) Euhedral sanidine in peralkaline trachyte, Buckland. (b) Subhedral sanidine in pitchstone, Springsure. (c and d) Euhedral sanidine in rhyolite, Peak Range. All sanidine crystals are unaltered but may be cut by fractures and/or cleavage planes. (e) Biotite in rhyolite, Peak Range. (f) Anorthoclase-plagioclase in trachyandesite, Peak Range. (g) Anorthoclase in metaluminous trachyte, Peak Range. (h) Fine-grained but crystalline groundmass of arfvedsonite (green), quartz, and K-feldspar (white), Peak Range. (i) K-feldspar in microgranite, Hillsborough. Parts of the crystal around the edges and fractures have sericite alteration, but the right and top of the crystal are fresh. All images except Figure 3h are taken in cross-polarized light.

Table 1. $^{40}Ar/^{39}Ar$ Results [a], in Order From North to South

Location & Sample #	Rock type & Material dated	Run #	Lab. #	# of steps	Plateau age ± 2σ (Ma)	Steps & % in Plateau	Integrated Age ± 2σ (Ma)	Ideogram Age ± 2σ (Ma)	Isochron Age ± 2σ (Ma)	40Ar/36Ar intercept	Comments
Mt Jukes, Hillsborough, BC-98	Granite, Kfeldspar	64	3746-01	8	33.8 ± 0.5	A-H (100)	33.8 ± 0.6	**33.6 ± 0.5** (n = 13)	NA	NA	Near-ideal flat spectra.
		64	3746-02		33.5 ± 0.5	B-J (96.9)	32.4 ± 0.5				
Dyke, Mt Britton, Nebo, DR13704	Porphyritic trachyte, Sa.	66	4062	10	Total fusion	NA	32.6 ± 0.4	32.6 ± 0.3 (n = 10)	**32.6 ± 0.4** (n = 10)	280 ± 80	Concordant results.
Wolfang Peak, North Peak Range, BC-89	Rhyolite, Sa.	66	4057	8	Total fusion	NA	30.4 ± 0.4	30.4 ± 0.3 (n = 8)	**30.3 ± 0.4** (n = 8)	320 ± 120	Concordant results.
	Rhyolite, Biotite	67	4058-01	8	30.8 ± 0.4	B-G (92.8)	30.9 ± 0.5	30.7 ± 0.4 (n = 13)	30.6 ± 0.4 (n = 17)	340 ± 50	Near-ideal flat spectra. Age is concordant with sanidine results.
	Rhyolite, Biotite	67	4058-02	9	30.4 ± 0.5	A-I (100)	30.2 ± 0.7				
Mt Pollux, North Peak Range, BC-88	Rhyolite, Sa.	61	3683	10	Total fusion	NA	30.7 ± 0.4	30.7 ± 0.4 (n = 9)	**30.7 ± 0.4** (n =10)	290 ± 20	Concordant results.
Lords Table Mountain, N. Peak Range, BC-90	Trachyandesite, feldspar	61	3731-01	13	30.4 ± 0.5	C-M (98.2)	30.5 ± 0.6	30.4 ± 0.5 (n = 25)	**30.4 ± 0.5** (n = 25)	350 ± 140	Flat spectra. Second grain did not release much gas.
		61	3731-02	13	30.9 ± 1.1	A-M (100)	30.9 ± 1.3				
Ropers Peak, South Peak Range, BC-95r	Peralkaline rock, GM	64	3737-01	11	28.5 ± 0.4	C-K (78.9)	29.1 ± 0.5	28.6 ± 0.4 (n = 16)	**28.6 ± 0.4** (n = 20)	317 ± 6	Minor recoil/excess Ar in low temperature steps.
		64	3737-02	11	28.7 ± 0.4	C-I (73.0)	29.5± 0.5				
Malvern Hill, South Peak Range, BC-94	Metaluminous trachyte, Ano.	61	3682-01	10	28.9 ± 0.4	A-J (100)	28.9 ± 0.5	28.9 ± 0.4 (n = 17)	**29.0 ± 0.4** (n = 19)	300 ± 200	Near-ideal flat spectra.
		61	3682-02	9	29.0 ± 0.4	A-I (100)	28.9 ± 0.5				
Plug, N. of Mt St Peter, Springsure, BC-71	Pitchstone, Sa.	70	4360	8	Total fusion	NA	28.1 ± 0.3	28.1 ± 0.3 (n = 8)	**28.1 ± 0.3** (n = 8)	320 ± 70	Concordant results.
'Hervey's Knob', Buckland, BC-57	Peralkaline trachyte, Sa.	61	3742	10	Total fusion	NA	27.3 ± 0.4	27.3 ± 0.4 (n = 10)	**27.3 ± 0.4** (n = 10)	310 ± 60	Concordant results.

[a]The best age estimate for each sample is highlighted. As isochron analysis identifies samples that have nonatmospheric initial argon, which can significantly affect the resulting age, we therefore use the isochron age as the best age estimate for each sample. For BC-98, the isochron is unavailable as all steps are highly radiogenic and all analyses cluster next to the *x* axis; instead, the mean-weighted age from the age probability density plot is used (the ideogram age) [*Deino and Potts*, 1992], as it weighs each analysis based on the calculated error, reducing the influence of imprecise outliers. Ideogram and isochron ages combine the results from all aliquots analyzed for that sample. GM = groundmass; Sa = sanidine; Ano = anorthoclase. The age and error calculation methods are as follows: plateau ages calculated as the mean weighted by inverse variance; plateau age errors are the standard error of the weighted mean; integrated ages calculated by isotopic recombination of steps; integrated age errors are the standard error of the weighted mean; ideogram ages calculated as the weighted mean; ideogram age errors are the standard error of the weighted mean; isochron ages are calculated from the $^{39}Ar/^{40}Ar$ intercept; isochron age errors are calculated using a York regression [*York*, 1969].

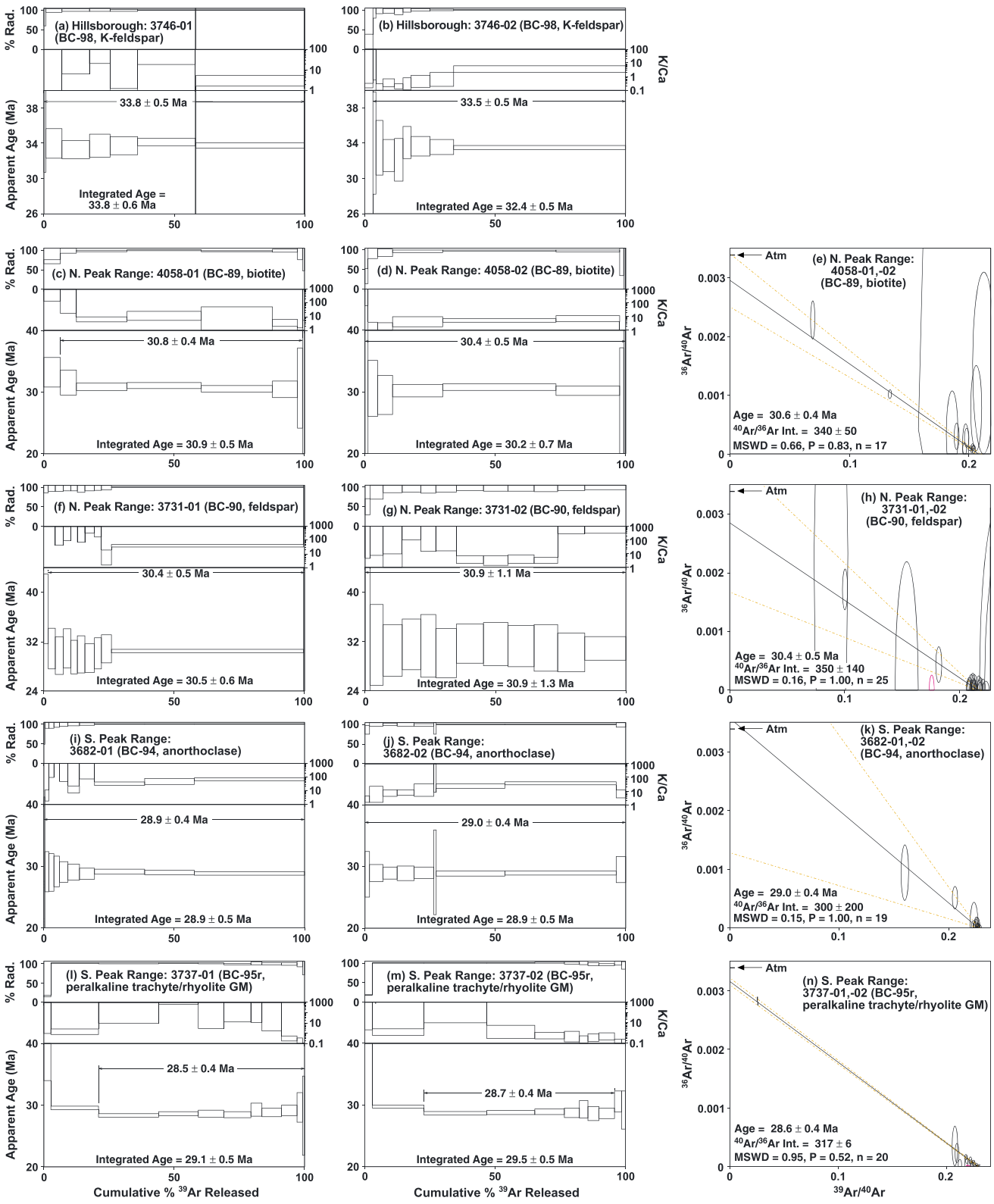

Figure 4. $^{40}Ar/^{39}Ar$ incremental-heating spectra, arranged from north to south. Two aliquots were analyzed per sample: (a and b) BC-98, (c and d) BC-89, (f and g) BC-90, (i and j) BC-94, and (l and m) BC-95r. (e, h, k, and n) Results from both aliquots were combined for isochron investigation. The exception is BC-98, where no isochron was able to be determined, as all analyses were highly radiogenic and yielded an insufficient spread of $^{36}Ar/^{40}Ar$ and $^{39}Ar/^{40}Ar$ values for isochron investigation. On the isochron diagrams, light brown dashed lines indicate 2σ error envelopes, and magenta ellipses indicate outliers not included in the age calculations.

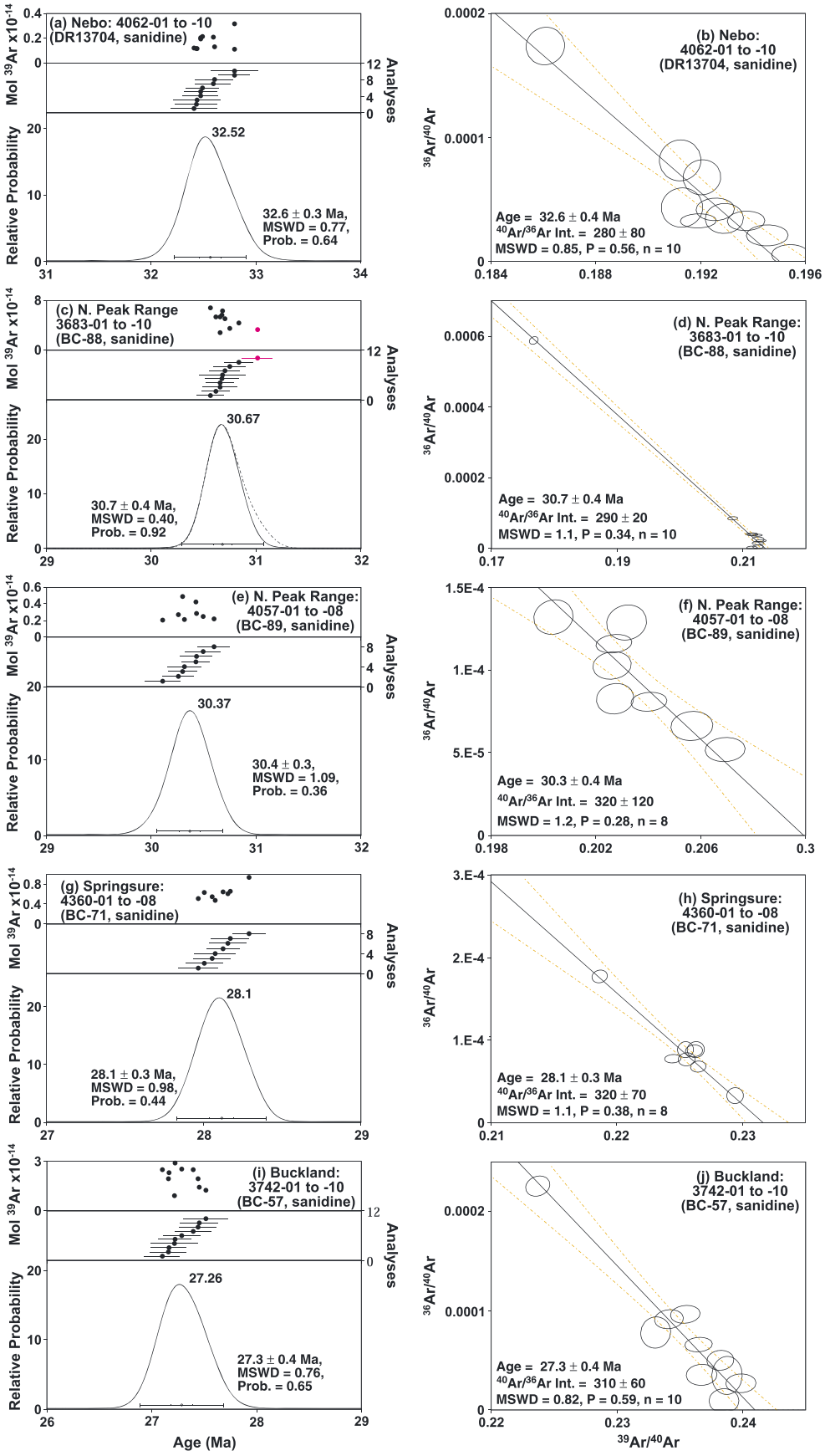

Figure 5. $^{40}Ar/^{39}Ar$ total-fusion results on sanidine, arranged from north to south. (left) The age probability spectra [*Deino and Potts*, 1992]. (right) The isochron for the corresponding sample. Symbols are as in Figure 4.

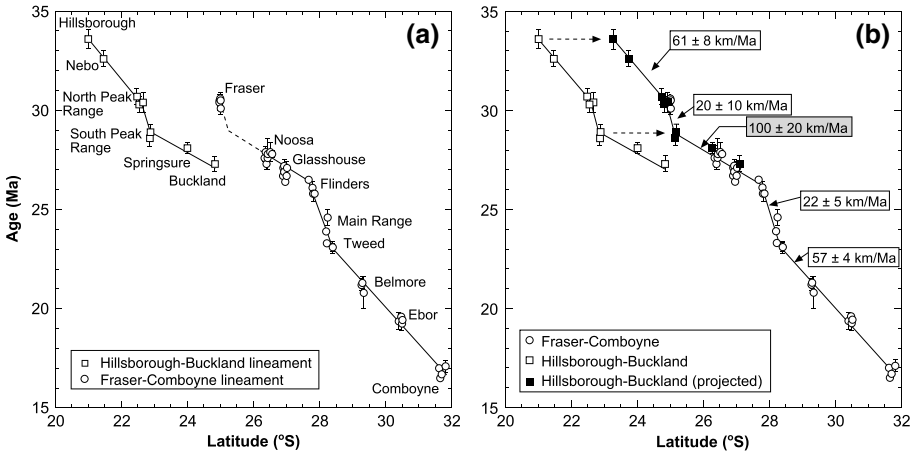

Figure 6. (a) $^{40}Ar/^{39}Ar$ ages for silicic volcanic rocks versus latitude, showing two abrupt and brief reductions in volcano migration rate, interspersed with a period of higher rate. Ages from this study on the Hillsborough-Buckland lineament are indicated by open squares; ages from the Fraser–Comboyne lineament (open circles) are from *Ashley et al*. [1995], *Cohen et al*. [2007], and *Knesel et al*. [2008]. Errors (2σ) are smaller than the symbols or are illustrated by error bars. (b) To directly compare ages from both lineaments and to calculate the Australian plate velocity, ages from the Hillsborough-Buckland lineament are projected 550 km east-southeast (filled squares), using a paleoplate azimuth of 018°. A York regression (Isoplot 3.0) [*Ludwig*, 2003] of the time periods 34–30, 30–29, 29–26, 26–23, and 23–16 Ma yields the northward component of Australian plate velocity, relative to a fixed hot spot reference frame, with 2σ uncertainties.

age, indicating that this sample yields a reliable age determination for the cooling of this rhyolite, with the best age estimate being the isochron age of 28.6 ± 0.4 Ma.

3.2. Total-Fusion Analyses

[13] For the five samples where sanidine was separated (from Nebo, Springsure, Buckland, and two from North Peak Range), between 8 and 10 aliquots of sanidine were analyzed by the total-fusion method. Individual aliquots usually consisted of single crystals, but when the crystals were small, two or three crystals were fused together (Table A2 in the supporting information). In all of these samples, there is excellent agreement between aliquots, with all analyses yielding a single high-probability cluster of ages (Figures 5a, 5c, 5e, 5g, and 5i). Inverse isochron ages were entirely compatible with the ages extracted from the probability density plots, and initial $^{40}Ar/^{36}Ar$ values were indistinguishable from modern-day atmosphere (Figures 5b, 5d, 5f, 5h, and 5j). These results indicate that the sanidine analyses are reliable estimates of the age of eruption, with no signs of argon loss due to reheating or alteration, and no signs of extraneous argon inherited from incomplete degassing of the magmas.

[14] A further cross-check of the age reliability is provided by comparison of sanidine (via total fusion) and biotite (via incremental heating) results for a peraluminous rhyolite BC-89 from the Northern Peak Range volcano. These independent analyses on different minerals analyzed via different heating techniques yield concordant ages, thus further demonstrating the reliability of the results. Therefore, based on the concordance of multiple aliquots per sample and the absence of substantial excess argon or argon loss from the material analyzed, we interpret that all samples yield reliable, precise, and reproducible ages that can be confidently interpreted as the timing of magma cooling in each of the five volcanoes studied (Figures 3 and 4 and Table 1).

4. Discussion

4.1. Speedometry of the Australian Plate

[15] The five volcanoes dated here form a lineament extending 440 km from Hillsborough in the north to Buckland in the south (Figure 2). This track is parallel but 500–600 km to the west of the volcanic track studied by *Cohen et al*. [2007] and *Knesel et al*. [2008]. The western volcanic trail therefore provides an independent test of our previous results and represents an important piece of the puzzle in our reconstruction of the motion of the Australian plate. Our results show that emplacement ages for the silicic rocks along the Hillsborough-Buckland lineament range from 33.6 ± 0.5 to 27.3 ± 0.4 Ma and, like their eastward counterparts, become progressively younger to the south (Figure 6a). Therefore, the new $^{40}Ar/^{39}Ar$ age data, while overlapping in time with the two oldest volcanic centers of the coastal track, extend the temporal coverage back to 33.6 ± 0.5 Ma and also fill a key time gap in the record previously constructed by *Cohen et al*. [2007] and *Knesel et al*. [2008]—the 30–27 Ma period between the Fraser and Noosa volcanoes (Figure 6a).

[16] It is presently unclear whether the two volcanic lineaments represent the products of two separate hot spots or if the two lineaments were fed from a single hot spot that spread out beneath the continental lithosphere, before reaching thinner zones or areas of lithospheric weakness such as major faults or sutures that allow the passage of magma to the surface [e.g., *Thompson and Gibson*, 1991; *Ebinger and Sleep*, 1998]. Resolving this issue is, however, not necessary for the purposes of tracking plate velocity, provided the plate is moving over a relatively stationary source or sources. To facilitate age comparison between the two lineaments, ages from the Hillsborough-Buckland volcanoes are projected 550 km east-southeast onto the corresponding part of the Fraser-Comboyne lineament (Figure 6b). This projection

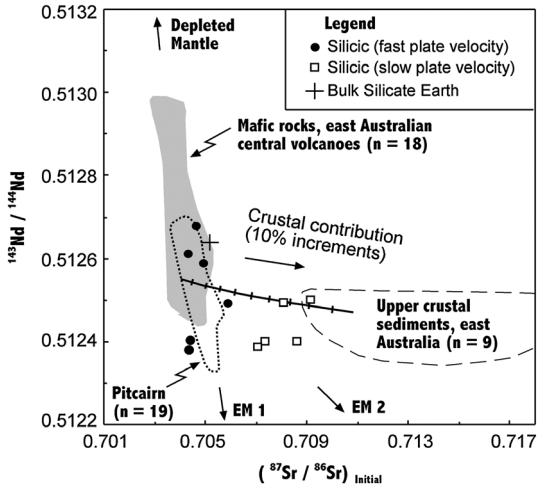

Figure 7. The plate velocity has a significant influence on the chemistry of the hot spot–derived volcanoes in eastern Australia. Silicic rocks erupted during fast velocities have isotopic values similar to mafic units, contrasting with the considerably more radiogenic $(^{87}Sr/^{86}Sr)_{initial}$ values for silicic rocks formed during periods of slow velocity. The mixing line shown is between a typical mafic lava (33753 from Tweed) and a typical upper crustal sediment from eastern Australia (38682, Neranleigh-Fernvale greywacke). East Australian isotopic data are from *Ewart* [1982] and *Ewart et al*. [1988, and references therein]; isotopic data from Pitcairn in the eastern Pacific [*Eisele et al*., 2002] are shown for comparison as a representative EM1 hot spot from an oceanic environment away from the influence of modern-day continental crust.

uses a paleoplate azimuth of 18°, which is compatible with the traces of the Tasmantid and Lord Howe seamount chains at this time (Figure 2).

[17] The combined data set (Figure 6) indicates that there were several abrupt changes in the rate of volcanic migration, with periods of markedly faster migration interspersed with times of much slower migration. Considering the errors on each age of 0.3–0.5 Ma and the <1 Ma duration of silicic activity at central volcanoes (Figure A1 in the supporting information), we conservatively estimate that the timings for velocity changes have errors of ±0.5 Ma. These results indicate that for most of the time period studied [from 34 to 30 (±0.5) Ma and from 23 to 16 (±0.5) Ma], the Australian plate velocity was 61 ± 8 and 57 ± 4 km/Ma, respectively, relative to a stationary hot spot reference frame (Figure 6). These velocities are indistinguishable from GPS-derived modern-day plate velocity of 54 km/Ma for the Australian plate over the east Australian hot spot [*Tregoning*, 2002]. We interpret this speed of ~60 km/Ma to be the steady state velocity of the Australian plate during the middle to late Cenozoic, when subduction was proceeding normally.

[18] The most pronounced deviation from this velocity of ~60 km/Ma is the abrupt reduction in volcanic migration to 22 ± 5 km/Ma experienced from 26 to 23 (±0.5) Ma (Figure 6). This reduction is accompanied by modifications in the volume, dimensions, and chemistry of volcanism, providing independent evidence for changes from fast to slow plate velocity, as outlined below.

[19] During periods of fast motion, relatively small hot spot–derived volcanoes were constructed in eastern Australia, with volumes ranging from 25 to 600 km^3 [*Duncan and McDougall*, 1989]. Silicic rocks erupted during these times of normal, relatively fast migration are dominated by metaluminous trachytes and peralkaline rhyolites. Sr, Nd, and Pb isotopic compositions from these units are similar to those of contemporaneous mantle-derived mafic magmas [*Ewart*, 1982; *Ewart et al*., 1988] (Figure 7). The geochemical and isotopic signatures reveal that during times of fast migration, small amounts of silicic magmas were generated via extensive fractional crystallization from mafic parental melts, producing extreme depletions and enrichments of compatible and incompatible elements, respectively (e.g., Sr < 10 ppm and Zr > 1000 ppm) [*Ewart et al*., 1985]. These magmas show only minor crustal contributions.

[20] On the other hand, volcanoes constructed during the 26–23 Ma period are considerably larger, with estimated original volumes of 4000 and 840 km^3 for Tweed and Main Range, respectively [*Duncan and McDougall*, 1989]; the volume of silicic rocks at these centers is also correspondingly higher. In addition, these silicic units are composed predominantly of peraluminous or high-silica rhyolites—rock types that are volumetrically insignificant or absent during times of fast migration. Isotopic analyses of rhyolites from the Tweed and Main Range centers yield radiogenic Pb and Sr compositions, indicating significant contributions from an upper crustal source [*Ewart*, 1982; *Ewart et al*., 1988] (Figure 7). Trace element compositions also indicate that the peraluminous rhyolites were generated via extensive crustal contamination of mantle-derived magmas, and the chemical compositions also demonstrate that these magmas underwent extensive modification by crystal fractionation (e.g., Eu/Eu* of 0.0023 for one flow from Tweed) [*Ewart et al*., 1985]. These time-space-volume-composition relations indicate that the 26–23 Ma period of slow migration provided more time for extensive melting of the crust above a stationary hot spot and for the construction of larger mafic shields than was possible during periods of more rapid plate motion.

[21] Further evidence for a change in plate velocity from 26 to 23 (±0.5) Ma is available from the concomitant westward offsets in the offshore Tasmantid and Lord Howe seamount chains [*Knesel et al*., 2008, Figure 2], as well as a westward excursion in the apparent polar wander path at this time [*McElhinny et al*., 1974]. These observations suggest that in addition to slowing down, the Australian plate also changed from a north northeasterly to a northwesterly trajectory during the 26–23 (±0.5) Ma period. The contemporaneous paleomagnetic excursion is particularly significant, as it indicates a change in plate direction that is independent of assumptions regarding the fixity of mantle hot spots, the nature of upper mantle flow, or the influence of lithospheric structure on the volcanic distribution. We therefore conclude that the volcanic products, through their age progressions and petrochemical characteristics, are faithful recorders of the changing northward velocity of the Australian plate [*Knesel et al*., 2008].

[22] Our new $^{40}Ar/^{39}Ar$ ages indicate that there was another brief reduction in Australian plate velocity, down to 20 ± 10 km/Ma, which occurred from 30 to 29 (±0.5) Ma (Figure 6). Volcanism during this earlier period of apparent slow migration has many similarities to volcanoes erupted during the 26–23 Ma event. Peak Range, where

silicic rocks were emplaced during the 30–29 Ma period, has an estimated original volume of 840 km^3, considerably larger than the 25–360 km^3 for other volcanoes erupted along the Hillsborough-Buckland lineament [*Duncan and McDougall*, 1989]. Peak Range also has an anomalously high volume and abundance of silicic plugs, many of which have the typical mineralogy of peraluminous crustal melts. Thus, the greater size of Peak Range compared to other volcanoes in central Queensland, combined with the abundance and probable crustal derivation of the rhyolites from this center, provides support for a reduction in Australian plate velocity from 30 to 29 Ma.

[23] This slowdown is contemporaneous with a proposed collision event in eastern New Guinea (Figure 8a). Tectonic reconstructions [*Quarles van Ufford and Cloos*, 2005; *Schellart et al*., 2006] indicate that thickened lithosphere entered along much of the length of the subduction zone at virtually the same time, rapidly shutting off subduction along the Papuan-Rennel trench. Introduction of thick lithosphere choked subduction, leading to collisional orogenesis [*Quarles van Ufford and Cloos*, 2005; *Schellart et al*., 2006] and influx of immature sediments into the Aure Trough, located in the south of New Guinea [*Quarles van Ufford and Cloos*, 2005].

[24] Between the two periods of slower plate velocity, our results reveal that the intervening period [29–26 (±0.5) Ma] has an unexpectedly fast plate velocity of 100 ± 20 km/Ma (Figure 6). Although this period of anomalously fast plate movement is independently recorded by the two longitudinally offset volcanic lineaments, i.e., Hillsborough-Buckland and Fraser-Comboyne (Figure 6), we note that a short period of anomalously fast Australian plate motion has not been identified in the corresponding seafloor-spreading record between the Australian and Antarctic plates [*Cande and Stock*, 2004a, 2004b]. The apparent lack of change in Australia-Antarctic spreading rate may be a case where changes in absolute plate motion did not cause modifications in relative plate motion, if both plates altered their relative motions in concert [e.g., *Wessel and Kroenke*, 2000]. Alternatively, the apparent absence of modified Australian-Antarctic spreading may instead suggest that the patterns of intraplate volcanism in eastern Australia are influenced by processes other than plate velocity, for example, changes in mantle flow in the southwest Pacific [*Sutherland et al*., 2012], or the influence of thick lithosphere on the time-space distribution of volcanism. We consider these options to be unlikely, given the corroboration of evidence from the volcano migration patterns, size, and chemistry, as well as the change in Australian Apparent Polar Wander Path. Nevertheless, the velocity of the Australian plate could be further constrained by detailed refinement of the Australian Apparent Polar Wander Path using modern paleomagnetic analysis of Australian intraplate magmatism (e.g., as suggested by *Vasconcelos et al*. [2008]), combined with additional geochronologic studies of the east Australian, Tasmantid, and Lord Howe hot spot chains. Further detailed work on seafloor spreading between Australia and Antarctica would be also highly beneficial to compare with the intraplate volcanic record but is beyond the scope of this contribution.

[25] The period of apparent accelerated plate motion up to 100 ± 20 km/Ma (Figure 6), if true, is significant because it exceeds the maximum steady state plate velocity of about 80 km/Ma (8 cm/yr) obtainable via slab pull for the oldest, densest slabs [*Goes et al*., 2008; *Stadler et al*., 2010]. Today, no plate exceeds this tectonic "speed limit"—especially not one carrying a continent; however, this has not always been the case. Velocities of 160 km/Ma or more are recorded for India from ~68 to 63 Ma [*Cande and Stegman*, 2011] and for parts of Gondwana from ~375 to 355 Ma and from ~340 to 320 Ma [*Meert et al*., 1993], underscoring the dynamic nature of plate tectonics. If the Australian plate did indeed accelerate to speeds of 100 km/Ma, it must have been accompanied by some drastic changes in tectonic architecture in the region.

4.2. Mechanisms for Fast Plate Motion

[26] To explain periods of anomalously fast plate velocities, especially for the Indian subcontinent, recent studies have drawn attention to the potential influence of plume-push forces [*Cande and Stegman*, 2011; *van Hinsbergen et al*., 2011], plume-induced thermomechanical erosion of the lithosphere [*Kumar et al*., 2007], or catastrophic slab penetration into the lower mantle [*Pysklywec et al*., 2003; *Goes et al*., 2008]. These three mechanisms are evaluated below with respect to the period of anomalously fast Australian plate velocity from 29 to 26 Ma.

[27] Plume push provides an additional driving force on plate motion via the buoyant uplift of the plate as a starting plume head impinges beneath the lithosphere [*Cande and Stegman*, 2011; *van Hinsbergen et al*., 2011]. At the same time, flood basalt volcanism is produced on the overlying plate [*Cande and Stegman*, 2011; *van Hinsbergen et al*., 2011]. In the case of accelerated Australian velocity from 29 to 26 (±0.5) Ma, this mechanism can be discounted because, at this time, there is no evidence for a large igneous province representing the impact of a starting plume under the Australian or nearby plates [*Coffin and Eldholm*, 1994]. The buoyancy flux provided by plume tails—such as those that would have produced the Tasmantid, Lord Howe, and east Australian hot spot volcanoes—provides insufficient forces to accelerate a plate [*Cande and Stegman*, 2011; *van Hinsbergen et al*., 2011].

[28] Reduction of the thickness of the lithosphere reduces drag forces on the base of a plate [*Kumar et al*., 2007]. This mechanism has been proposed to explain the rapid Cretaceous velocity of India, which presently has a continental keel less than 100 km thick [*Kumar et al*., 2007]. Seismic tomography, however, indicates that Australia still retains an ancient sublithospheric mantle root up to 200 km thick [*Kumar et al*., 2007; *Fishwick and Rawlinson*, 2012]. There is also no mechanism to substantially thin the Australian lithosphere in the 29–26 Ma interval. For instance, tectonic thinning is precluded by the stable intraplate setting at the time. Likewise, thermomechanical thinning of the lithosphere via a starting plume head [*Kumar et al*., 2007] can be ruled out due to the lack of an accompanying large igneous province [*Coffin and Eldholm*, 1994]. These factors indicate that thinning of the lithosphere did not play a part in the accelerated Australian plate motion from 29 to 26 Ma.

[29] Geodynamic models show that catastrophic avalanching of a formerly stagnant slab through the transition zone increases the velocity of the subducting plate [*Zhong and Gurnis*, 1995; *Pysklywec et al*., 2003; *Goes et al*., 2008]. Rapid slab penetration into the lower mantle is favored by near-vertical sinking and piling up of the slab at the transition

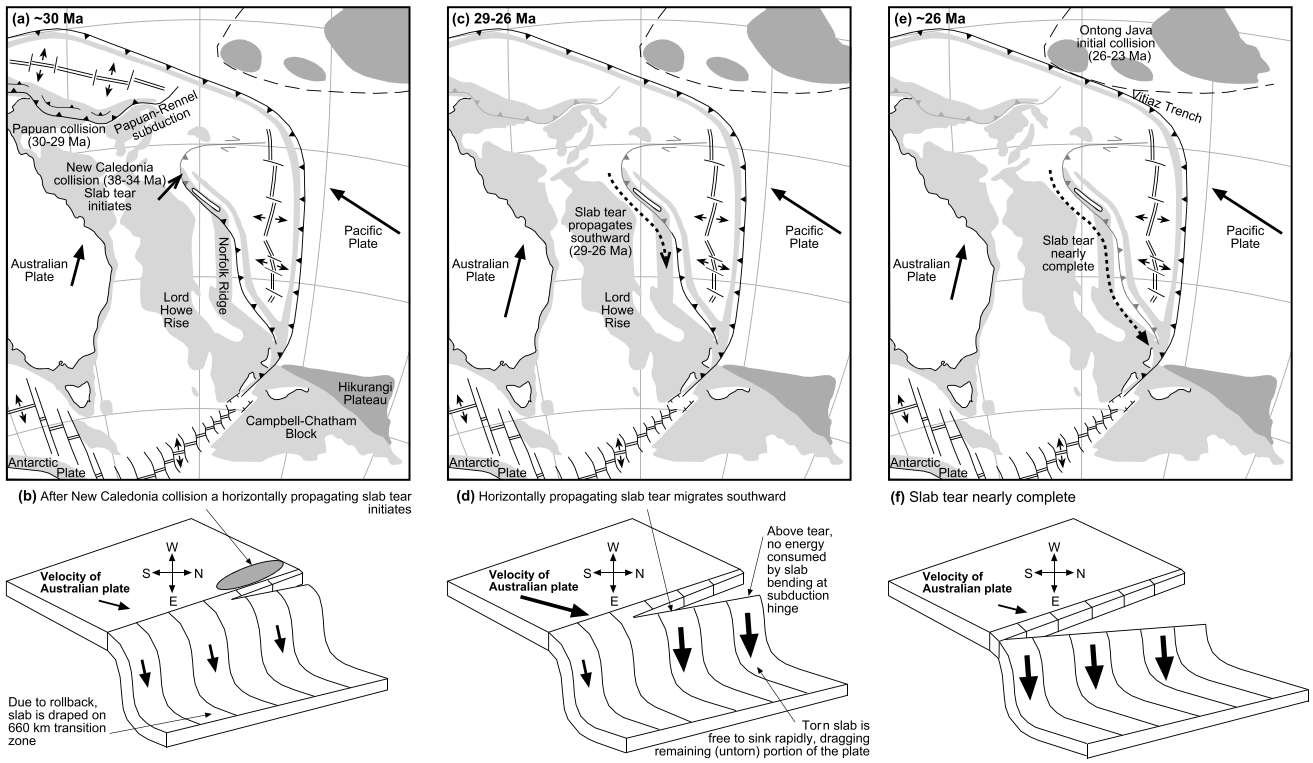

Figure 8. Plate-tectonic reconstructions after *Schellart et al*. [2006] and schematic models for the southwest Pacific at 30 Ma, 29–26 Ma, and ~26 Ma. The New Caledonia subduction system was between 2000 and 2500 km long [*Schellart et al*., 2006], comprising approximately 30% of the subduction boundary of the Australian plate. Changes in the force balance along this subduction system due to slab tearing around New Caledonia would therefore exert considerable influence on the velocity of the Australian plate.

zone, followed by catastrophic gravitational sinking through the 660 km discontinuity [*Goes et al*., 2008]. This scenario is not consistent with the characteristics of subduction on the margins of the Australian plate during the Oligocene. In particular, the New Caledonia subduction system underwent rollback amounting to 50–75% of the total plate convergence [*Schellart et al*., 2009], thus draping the slab approximately horizontally over the transition zone [*Schellart*, 2011]. This geometry is confirmed by seismic tomographic images of the detached slab, showing a broad and flat fossil slab at ~1100 km depth [*Schellart et al*., 2009]. This present-day depth of the fossil slab also indicates gradual sinking through the lower mantle at rates of ~15 km/Ma (1.5 cm/yr) [*Schellart et al*., 2009; *Schellart and Spakman*, 2012], as opposed to catastrophic and rapid penetration through the transition zone. Slab avalanching through the Indonesian (northwestern) segment of the Australian plate may be a possibility, but there is no known evidence in the geologic record to suggest that this process occurred from 29 to 26 Ma [*Hall*, 2002].

[30] The 29–26 (±0.5) Ma period of accelerated plate velocity, however, does correlate with an interpreted slab tear event in the southwest Pacific (Figures 8c and 8d). At 30 Ma, oblique plate convergence was accommodated by westward dipping subduction of the Pacific plate along the Tonga-Kermadec subduction zone, combined with northeastward dipping subduction of the Australian plate along the New Caledonia–Northland and Papuan-Rennel subduction zones [*Hall*, 2002; *Schellart et al*., 2006] (Figure 8). Introduction of thick continental lithosphere of the Norfolk Ridge into the trench (Figure 8c) eventually choked subduction around New Caledonia and led to ophiolite obduction from 38 to 34 Ma [*Cluzel et al*., 2001; *Schellart et al*., 2006]. As convergence continued, a subhorizontally propagating tear developed in the northern part of the slab at ~30 Ma [*Schellart et al*., 2006, 2009] (Figure 8b). The age of the proposed tearing is constrained by the commencement of magmatism in New Caledonia from ~27 to 23 Ma [*Cluzel et al*., 2005], which resulted from upwelling of hot asthenosphere through the gap in the slab, likely a few million years after the tear had become fully established [*Cluzel et al*., 2005; *Schellart*, 2007]. This tear then enabled the northern portion of the slab to sink unhindered into the mantle (Figure 8d).

[31] Whether the changes in subduction following obduction and subsequent initiation of slab tearing in the New Caledonia region can explain the fast motion of the Australian plate is uncertain and requires scrutiny through analogue or computational analysis of subducting slabs. Nevertheless, it is intriguing to note that this fast motion continued until the southward propagating tear culminated with the detachment of the slab in the southern part of the subduction zone (Figure 8) following the arrival of buoyant, thick lithosphere of the Norfolk Ridge and Lord Howe Rise, which choked subduction and triggered obduction around Northland, New Zealand, at either 26 or 25 Ma [*Mortimer et al*., 2003; *Schellart et al*., 2009]. The remaining portion of the slab then detached from the Australian plate and sank through the mantle (Figure 8f). Today, the detached slab has been imaged as an

approximately flat-lying fast seismic anomaly ~2200 km long by 600–900 km wide located at ~1100 km depth, beneath the central Tasman Sea [*Schellart et al*., 2009].

[32] At 26 ± 0.5 Ma, motion of the Australian plate abruptly slowed to 22 ± 5 km/Ma (Figure 6). The ensuing brief period of greatly reduced Australian plate motion was accompanied by offsets in the Tasmantid and Lord Howe seamount tracks on the Australian plate [*Knesel et al*., 2008] (Figure 2), as well as in the Hawaiian, Louisville, Caroline, and Cobb tracks in the Pacific [*Wessel and Kroenke*, 2008]. Relative motion between the Pacific and Antarctic plates also changed at this time [*Croon et al*., 2008]. Reconstruction of seafloor flow lines, which place the Ontong Java plateau near the Vitiaz trench in the late Oligocene [*Kroenke et al*., 2004], indicates that these features reflect deflection of both the Australian and Pacific plates as the extraordinarily thick plateau began colliding with the Australian plate [*Knesel et al*., 2008]. Therefore, while the final stage of slab tearing and detachment along the New Caledonia–Northland subduction zone may have contributed to the slowdown at 26 ± 0.5 Ma, the onset of oblique collision with the immense Ontong Java plateau appears to have been the driver for much of the rapid change in the motion and plate boundaries at this time. With the ensuing initiation of southward dipping subduction north of New Guinea by 23 ± 0.5 Ma [*Quarles van Ufford and Cloos*, 2005], Australia returned to its normal north-northeastward trajectory (Figures 2 and 6).

5. Conclusions

[33] Nine new $^{40}Ar/^{39}Ar$ ages from five east Australian intraplate volcanoes further indicate that the time-space migration of volcanism was not constant during the Cenozoic. Rates of circa 60 km/Ma prevailed from 34 to 30 (±0.5) and from 23 to 16 (±0.5) Ma but were interspersed with periods of much slower migration (circa 20 km/Ma) from 30 to 29 (±0.5) and from 26 to 23 (±0.5) Ma. These changes in volcanic migration rate correlate with modifications in volcano size and chemistry, as well as a change in Australian Apparent Polar Wander Path for the 26–23 Ma event, indicating substantial modifications in Australian plate velocity relative to a stationary mantle hot spot reference frame. The periods of slower velocity correlate to collisions in New Guinea and Ontong Java, respectively. The $^{40}Ar/^{39}Ar$ results also indicate a period of anomalously fast Australian plate velocity, of 100 ± 20 km/Ma, prevailed from 29 to 26 (±0.5) Ma. The velocity during this 3 Myr window exceeds the maximum steady state plate speed obtainable via slab pull in the upper mantle. The most significant tectonic change that temporally corresponds with this 29–26 (±0.5) Ma anomalously fast period is a slab tear event that occurred along the New Caledonia subduction zone on the northeastern Australian plate margin. However, whether such slab tearing and sinking can in fact lead to anomalously fast plate motion is unclear and requires further examination, using analogue or computational models of subduction. In any case, the extreme brevity of these plate velocity changes further highlights the rapid nature of tectonic change at subduction margins and the considerable influence of plate-boundary forces on the absolute velocities of the Earth's tectonic plates [*Hall*, 2002; *Schellart et al*., 2006; *Knesel et al*., 2008].

[34] **Acknowledgments.** We thank A. Ewart, A. Mostert, and D. Thiede for discussions; S. Cande, J. Geldmacher, and D. Phillips for comments on previous versions of the manuscript; E. Sobel and an anonymous reviewer for positive and helpful reviews of the article; T. Ehlers for editorial handling; the Queensland National Parks and Wildlife Service and various landowners for permitting fieldwork; and staff at Australian Museum, especially F. L. Sutherland and I. Graham, for providing a sample from the Nebo volcano. D. Thiede is also thanked for valuable assistance during analytical work. Construction of the University of Queensland Argon Geochronology in Earth Sciences laboratory (UQ-AGES) was partially funded by the Australian Research Council; this project was funded through UQ-AGES contract research. The conceptual idea for this study was developed by P.M. V., K.M.K., and B.E.C. Field work, sample analysis, and data interpretation were undertaken by B.E.C. under the supervision of P.M.V. and K.M.K. The manuscript and figures were created by B.E.C, in discussion with all authors. All authors contributed to the scientific ideas and writing of the manuscript.

References

Ashley, P. M., R. A. Duncan, and C. A. Feebrey (1995), Ebor Volcano and Crescent Complex, northeastern New South Wales: Age and geological development, *Aust. J. Earth Sci.*, *42*, 471–480.

Cande, S. C., and D. R. Stegman (2011), Indian and African plate motions driven by the push force of the Réunion plume head, *Nature*, *475*, 47–52, doi:10.1038/nature10174.

Cande, S. C., and J. M. Stock (2004a), Cenozoic reconstructions of the Australia–New Zealand–South Pacific sector of Antarctica, in *The Cenozoic Southern Ocean: Tectonics, Sedimentation, and Climate Change Between Australia and Antarctica*, edited by N. F. Exon, J. P. Kennett, and M. Malone, pp. 5–17, AGU, Washington, D. C.

Cande, S. C., and J. M. Stock (2004b), Pacific-Antarctic-Australia motion and the formation of the Macquarie Plate, *Geophys. J. Int.*, *157*, 399–414, doi:10.1111/j.1365-246X.2004.02224.x.

Cluzel, D., J. C. Aitchison, and C. Picard (2001), Tectonic accretion and underplating of mafic terranes in the late Eocene intraoceanic fore-arc of New Caledonia (Southwest Pacific): Geodynamic implications, *Tectonophysics*, *340*, 23–59.

Cluzel, D., D. Bosch, J.-L. Paquette, Y. Lemennicier, P. Montjoie, and R.-P. Ménot (2005), Late Oligocene post-obduction granitoids of New Caledonia: A case for reactivated subduction and slab break-off, *Isl. Arc*, *14*, 254–271.

Coffin, M. F., and O. Eldholm (1994), Large igneous provinces: Crustal structure, dimensions, and external consequences, *Rev. Geophys.*, *32*(1), 1–36.

Cohen, B. E., P. M. Vasconcelos, and K. M. Knesel (2007), $^{40}Ar/^{39}Ar$ constraints on the timing of Oligocene intraplate volcanism in southeast Queensland, *Aust. J. Earth Sci.*, *54*(1), 105–125, doi:10.1080/08120090600981483.

Cohen, B. E., K. M. Knesel, P. M. Vasconcelos, D. S. Thiede, and J. M. Hergt (2008), $^{40}Ar/^{39}Ar$ constraints on the timing and origin of Miocene leucitite volcanism in southeastern Australia, *Aust. J. Earth Sci.*, *55*, 407–418, doi:10.1080/08120090701769514.

Cowley, S., P. Mann, M. F. Coffin, and T. H. Shipley (2004), Oligocene to recent tectonic history of the Central Solomon intra-arc basin as determined from marine seismic reflection data and compilation of onland geology, *Tectonophysics*, *389*, 267–307, doi:10.1016/j.tecto.2004.01.008.

Croon, M. B., S. C. Cande, and J. M. Stock (2008), Revised Pacific-Antarctic plate motions and geophysics of the Menard Fracture Zone, *Geochem. Geophys. Geosyst.*, *9*, Q07001, doi:10.1029/2008GC002019.

Deino, A., and R. Potts (1992), Age-probability spectra for examination of single-crystal $^{40}Ar/^{39}Ar$ dating results: Examples from Olorgesailie, southern Kenya Rift, *Quat. Int.*, *13/14*, 47–53.

Duncan, R. A., and I. McDougall (1989), Volcanic time-space relationships, in *Intraplate Volcanism in Eastern Australia and New Zealand*, edited by R. W. Johnson, pp. 43–53, Cambridge Univ. Press, Cambridge.

Ebinger, C. J., and N. H. Sleep (1998), Cenozoic magmatism throughout east Africa resulting from impact of a single plume, *Nature*, *395*, 788–791.

Eisele, J., M. Sharma, S. J. G. Galer, J. Blichert-Toft, C. W. Devey, and A. W. Hofmann (2002), The role of sediment recycling in EM-1 inferred from Os, Pb, Hf, Nd, Sr isotope and trace element systematics of the Pitcairn hotspot, *Earth Planet. Sci. Lett.*, *196*, 197–212.

Ewart, A. (1982), Petrogenesis of the tertiary anorogenic volcanic series of southern Queensland, Australia, in the light of trace element geochemistry and O, Sr and Pb isotopes, *J. Petrol.*, *23*(3), 344–382.

Ewart, A., B. W. Chappell, and R. W. Le Maitre (1985), Aspects of the mineralogy and chemistry of the intermediate-silicic Cainozoic volcanic rocks of eastern Australia. Part 1: Introduction and geochemistry, *Aust. J. Earth Sci.*, *32*, 359–382.

Ewart, A., B. W. Chappell, and M. A. Menzies (1988), An overview of the geochemical and isotopic characteristics of eastern Australian Cainozoic volcanic provinces, in *Oceanic and Continental Lithosphere:*

Similarities and Differences, J. Petrol. Spec. Publ., edited by M. A. Menzies and K. Cox, pp. 255–274, Oxford Univ. Press, New York.

Fishwick, S., and N. Rawlinson (2012), 3-D structure of the Australian lithosphere from evolving seismic datasets, *Aust. J. Earth Sci.*, *59*(6), 809–826, doi:10.1080/08120099.2012.702319.

Fleck, R. J., J. F. Sutter, and D. H. Elliot (1977), Interpretation of discordant $^{40}Ar/^{39}Ar$ age-spectra of Mesozoic tholeiites from Antarctica, *Geochim. Cosmochim. Acta*, *41*, 15–32.

Goes, S., F. A. Capitanio, and G. Morra (2008), Evidence of lower-mantle slab penetration phases in plate motions, *Nature*, *451*, 981–984, doi:10.1038/nature06691.

Hall, R. (2002), Cenozoic geological and plate tectonic evolution of SE Asia and the SW Pacific: Computer-based reconstructions, model and animations, *J. Asian Earth Sci.*, *20*, 353–431.

Knesel, K. M., B. E. Cohen, P. M. Vasconcelos, and D. S. Thiede (2008), Rapid change in drift of the Australian plate records collision with Ontong Java plateau, *Nature*, *454*, 754–757, doi:10.1038/nature07138.

Kroenke, L. W., P. Wessel, and A. Sterling (2004), Motion of the Ontong Java Plateau in the hot-spot frame of reference: 122 Ma–present, in *Origin and Evolution of the Ontong Java Plateau*, edited by J. G. Fitton et al., pp. 9–20, Geol. Soc. of London, London.

Kuiper, K. F., A. Deino, F. J. Hilgen, W. Krijgsman, P. R. Renne, and J. R. Wijbrans (2008), Synchronizing rock clocks of Earth history, *Science*, *320*, 500–504, doi:10.1126/science.1154339.

Kumar, P., X. Yuan, M. R. Kumar, R. Kind, X. Li, and R. K. Chadha (2007), The rapid drift of the Indian tectonic plate, *Nature*, *449*, 894–897, doi:10.1038/nature06214.

Lee, J.-Y., K. Marti, J. P. Severinghaus, K. Kawamura, H.-S. Yoo, J. B. Lee, and J. S. Kim (2006), A redetermination of the isotopic abundances of atmospheric Ar, *Geochim. Cosmochim. Acta*, *70*, 4507–4512, doi:10.1016/j.gca.2006.06.1563.

Ludwig, K. R. (2003), Isoplot version 3.00: A Geochronological Toolkit for Microsoft Excel, *Berkeley Geochronology Centre Special Publication 4*.

McElhinny, M. W., B. J. J. Embleton, and P. Wellman (1974), A synthesis of Australian Cenozoic palaeomagnetic results, *Geophys. J. R. Astron. Soc.*, *36*, 141–151.

Meert, J. G., R. Van der Voo, C. M. Powell, Z.-X. Li, M. W. McElhinny, Z. Chen, and D. T. A. Symons (1993), A plate-tectonic speed limit?, *Nature*, *363*, 216–217.

Min, K., R. Mundil, P. R. Renne, and K. R. Ludwig (2000), A test for systematic errors in $^{40}Ar/^{39}Ar$ geochronology through comparison with U/Pb analysis of a 1.1-Ga rhyolite, *Geochim. Cosmochim. Acta*, *64*(1), 73–89.

Mortimer, N., R. H. Herzer, N. W. Walker, A. T. Calvert, D. Seward, and C. H. Chaproniere (2003), Cavalli Seamount, Northland Plateau, SW Pacific Ocean: A Miocene metamorphic core complex?, *J. Geol. Soc. London*, *160*, 971–983.

Müller, R. D., J.-Y. Royer, and L. A. Lawver (1993), Revised plate motions relative to the hotspots from combined Atlantic and Indian Ocean hotspot tracks, *Geology*, *21*, 275–278.

Petterson, M. G., C. R. Neal, J. J. Mahoney, L. W. Kroenke, A. D. Saunders, T. L. Babbs, R. A. Duncan, D. Tolia, and B. McGrail (1997), Structure and deformation of north and central Malaita, Solomon Islands: Tectonic implications for the Ontong Java Plateau–Solomon arc collision, and for the fate of oceanic plateaus, *Tectonophysics*, *283*, 1–33.

Petterson, M. G., et al. (1999), Geological-tectonic framework of Solomon Islands, SW Pacific: Crustal accretion and growth within an intra-oceanic setting, *Tectonophysics*, *301*, 35–60.

Pysklywec, R. N., J. X. Mitrovica, and M. Ishii (2003), Mantle avalanche as a driving force for tectonic reorginization in the southwest Pacific, *Earth Planet. Sci. Lett.*, *209*, 29–38, doi:10.1016/S0012-821X(03)00073-6.

Quarles van Ufford, A., and M. Cloos (2005), Cenozoic tectonics of New Guinea, *AAPG Bull.*, *89*(1), 119–140, doi:10.1306/08300403073.

Ray, J. S., J. J. Mahoney, R. A. Duncan, J. Ray, P. Wessel, and D. F. Naar (2012), Chronology and geochemistry of lavas from the Nazca Ridge and Easter Seamount Chain: An ~30 Myr hotspot record, *J. Petrol.*, *53*(7), 1414–1448, doi:10.1093/petrology/egs021.

Renne, P. R., C. C. Swisher, A. Deino, D. B. Karner, T. L. Owens, and D. J. De Paolo (1998), Intercalibration of standards, absolute ages and uncertainties in $^{40}Ar/^{39}Ar$ dating, *Chem. Geol.*, *145*, 117–152.

Renne, P. R., R. Mundil, G. Balco, K. Min, and K. R. Ludwig (2010), Joint determination of ^{40}K decay constants and $^{40}Ar^*/^{40}K$ for the Fish Canyon sanidine standard, and improved accuracy for $^{40}Ar/^{39}Ar$ geochronology, *Geochim. Cosmochim. Acta*, *74*, 5349–5367, doi:10.1016/j.gca.2010.06.017.

Schellart, W. P. (2007), North-eastward subduction followed by slab detachment to explain ophiolite obduction and early Miocene volcanism in Northland, New Zealand, *Terra Nova*, *19*, 211–218, doi:10.1111/j.1365-3121.2007.00736.x.

Schellart, W. P. (2011), A subduction zone reference frame based on slab geometry and subduction partitioning of plate motion and trench migration, *Geophys. Res. Lett.*, *38*, L16317, doi:10.1029/2011GL048197.

Schellart, W. P., and W. Spakman (2012), Mantle constraints on the plate tectonic evolution of the Tonga-Kermadec-Hikurangi subduction zone and the South Fiji Basin region, *Aust. J. Earth Sci.*, *59*(6), 933–952, doi:10.1080/08120099.2012.679692.

Schellart, W. P., G. S. Lister, and V. G. Toy (2006), A Late Cretaceous and Cenozoic reconstruction of the Southwest Pacific region: Tectonics controlled by subduction and slab rollback processes, *Earth Sci. Rev.*, *76*, 191–233, doi:10.1016/j.earscirev.2006.01.002.

Schellart, W. P., B. L. N. Kennett, W. Spakman, and M. Amaru (2009), Plate reconstructions and tomography reveal a fossil lower mantle slab below the Tasman Sea, *Earth Planet. Sci. Lett.*, *278*, 143–151, doi:10.1016/j.epsl.2008.11.004.

Sdrolias, M., R. D. Müller, and C. Gaina (2003), Tectonic evolution of the southwest Pacific using constraints from backarc basins, in *Evolution and Dynamics of the Australian Plate*, edited by R. R. Hillis and R. D. Müller, pp. 343–359, Geol. Soc. Aust. Spec. Publ., vol. 22, and Geol. Soc. Am. Spec. Pap., vol. 372, Sydney.

Sharp, W. D., and D. A. Clague (2006), 50-Ma initiation of Hawaiian-Emperor bend records major change in Pacific plate motion, *Science*, *313*, 1281–1284, doi:10.1126/science.1128489.

Stadler, G., M. Gurnis, C. Burstedde, L. C. Wilcox, L. Alisic, and O. Ghattas (2010), The dynamics of plate tectonics and mantle flow: From local to global scales, *Science*, *329*, 1033–1038, doi:10.1126/science.1191223.

Steiger, R. H., and E. Jäger (1977), Subcommission on geochronology: Convention on the use of decay constants in geo- and cosmochemistry, *Earth Planet. Sci. Lett.*, *36*, 359–362.

Sutherland, F. L., I. T. Graham, S. Meffre, H. Zwingmann, and R. E. Pogson (2012), Passive-margin prolonged volcanism, East Australian Plate: Outbursts, progressions, plate controls and suggested causes, *Aust. J. Earth Sci.*, *59*, 983–1005, doi:10.1080/08120099.2012.688293.

Thompson, R. N., and S. A. Gibson (1991), Subcontinental mantle plumes, hotspots and pre-existing thinspots, *J. Geol. Soc. London*, *148*, 973–977.

Tregoning, P. (2002), Plate kinematics in the western Pacific derived from geodetic observations, *J. Geophys. Res.*, *107*(B1), 2020, doi:10.1029/2001JB000406.

van Hinsbergen, D. J. J., B. Steinberger, P. V. Doubrovine, and R. Gassmöller (2011), Accelleration and deceleration of India-Asia convergence since the Cretaceous: Roles of mantle plumes and continental collision, *J. Geophys. Res.*, *116*, B06101, doi:10.1029/2010JB008051.

Vasconcelos, P. M., K. M. Knesel, B. E. Cohen, and J. A. Heim (2008), Geochronology of the Australian Cenozoic: A history of tectonic and igneous activity, weathering, erosion, and sedimentation, *Aust. J. Earth Sci.*, *55*(6/7), 865–914, doi:10.1080/08120090802120120.

Wellman, P., and I. McDougall (1974), Cainozoic igneous activity in eastern Australia, *Tectonophysics*, *23*, 49–65.

Wessel, P., and L. W. Kroenke (2000), Ontong Java Plateau and late Neogene changes in Pacific plate motion, *J. Geophys. Res.*, *105*(B12), 28,255–28,277.

Wessel, P., and L. W. Kroenke (2008), Pacific absolute plate motion since 145 Ma: An assessment of the fixed hot spot hypothesis, *J. Geophys. Res.*, *113*, B06101, doi:10.1029/2007JB005499.

Wessel, P., and L. W. Kroenke (2009), Observations of geometry and ages constrain relative motion of Hawaii and Louisville plumes, *Earth Planet. Sci. Lett.*, *284*, 467–472, doi:10.1016/j.epsl.2009.05.012.

Whittaker, J. M., R. D. Müller, G. Leitchenkov, H. Stagg, M. Sdrolias, C. Gaina, and A. Goncharov (2007), Major Australian-Antarctic plate reorganization at Hawaiian-Emperor bend time, *Science*, *318*, 83–86, doi:10.1126/science.1143769.

York, D. (1969), Least squares fitting of a straight line with correlated errors, *Earth Planet. Sci. Lett.*, *5*, 320–324.

Zhong, S., and M. Gurnis (1995), Mantle convection with plates and mobile, faulted plate margins, *Science*, *267*, 838–843.